PROPAGATION MEASUREMENTS USING SYNTHETIC APERTURE RADAR TECHNIQUES

T. Brook, P.F. Driessen, R.L. Kirlin

Department of Electrical and Computer Engineering
University of Victoria, Victoria, B.C., Canada V8W 1P6
peter@ece.uvic.ca http://www.ece.uvic.ca/peter/

Abstract: **Measured complex impulse responses at 1 GHz in mountainous terrain is processed as data from a synthetic aperture array, thus identifying the power reflected from the terrain at various bearings and distances from the receiver. Thus we assign a reflection coefficient and corresponding intensity to each of the triangular faces in the terrain data base. A 3-D plot of the terrain thus shows a "radio eyes" (bistatic radar) view of the mountainside.**

The reflection coefficient from each triangular face has also been determined theoretically using the generalized Lambertian rough surface scattering model of [4], and agrees well with the measured data (correlation coefficient 0.88).

Using this scattering model, we have estimated the impulse response (multipath delay profile) in mountainous terrain directly from topographical map data. The estimated impulse response agrees well with the measured response, thus establishing confidence in the model. Such estimates can help to select cell site locations and antenna configurations to minimize the delay spread.

I. INTRODUCTION

Our objective is to use topographic data bases to obtain cell site coverage maps which includes the multipath delay profile as well as the signal strength. Such maps may be used to predict the signal quality (bit error rate) or outage probability as a function of receiver location for digital cellular radio systems. The best cell layout may thus be determined by computer experiment rather than actual measurements.

This objective may be achieved by using a scattering model to establish a reflection coefficient to each triangular face (surface element) in the terrain data base, and tracing all rays from transmitter via each face to receiver. The reflection coefficient will depend on the angles of incidence and reflection, surface roughness and other parameters of the surface element, and may be characterized statistically [1][2][3].

A generalized Lambertian scattering model defined by Oren [4] is found to yield results which correspond with measured data in Vancouver, Canada. The topography includes steep mountain slopes to the north, causing significant power in long delay multipaths at 1 GHz [5][6][7][8]. The data was recorded at 100 locations forming a crossed synthetic aperture array, using a 10 Mb/sec sliding correlator, thereby yielding complex impulse responses for the multipath channel with time resolution of 50 nsec.

The data was processed using minimum variance distortionless response (MVDR, also referred to as Linear Constrained Minimum Variance (LCMV)) as described in [5][12]. Details of the cross-array signal processing are given in Appendix A. The LCMV angle versus distance results are converted into distance versus distance results plots to coordinate the actual points of reflection with the topographical data.

II. SCATTERING MODELS

The terrain is represented by a geographical data base of elevations z as a as a function of position (x, y). The points (x, y, z) define the vertices of triangular regions or patches of terrain S_k with known orientation. Following [5][6], the channel impulse reponse is

$$h(t) = \sum_k \rho_k e^{j\phi_k} \delta(t - \tau_k) \tag{1}$$

where $\tau_k = (r_{TS_k} + r_{S_kR})/c$ is the absolute delay of the path from T via the k-th scatterer S_k to R, and

$$|\rho_k|^2 = \frac{\lambda^2}{(4\pi)^3} \frac{\sigma_k^0 dA_k}{r_{TS_k}^2 r_{S_kR}^2} \tag{2}$$

where σ_k^0 is the normalized scattering cross-section of the patch S_k with area dA_k. σ_k^0 is related to the albedo R of S_k. In practice, the contributions to ρ_k from all patches for which τ_k is constant within the resolution (bandwidth) of the system are summed together.

For a mountainous region, all S_k are modelled as rough surface scatterers or diffuse reflectors. We consider both the Lambertian scattering model and the generalized non-Lambertian model of [4] for the S_k.

0-7803-3157-5/96 $5.00 © 1996 IEEE

Other models for σ_k^0 are described in [9][10][11]. The Lambertian model assumes

$$\sigma_k^0 = \frac{R}{\pi} cos\theta_{i,k} \tag{3}$$

where $\theta_{i,k}$ is the angle of incidence relative to the normal vector $\hat{n_k}$ which defines the orientation of the S_k. R is assumed constant for all S_k. For fixed $\theta_{i,k}$, the reflectance does not change as the observer moves.

The generalized model of [4] (Oren model) assumes that each S_k with area dA_k is comprised of many Lambertian facets da with different orientations θ_a (V-cavity model, Figure 1a) such that $\lambda^2 \ll da \ll dA$. This assumption is appropriate for S_k on mountain slopes with vertices on a 100 meter grid and a wavelength $\lambda \simeq 33$ cm. For isotropic surface roughness, the Oren model assumes that the fraction of area that is occupied with facets with orientation θ_a with respect to $\hat{n_k}$ is Gaussian distributed with mean 0 and variance σ^2. In this model, the reflectance of the surface increases as the observer approaches the source direction. This may be seen by considering a single V-cavity (Figure 1b) with two Lambertian facets and an arbitrary source direction θ_i. The difference in reflectance between the brighter and darker of the two facets increases with θ_i. As the observer moves towards the source direction ($\theta_r \rightarrow \theta_i$), the fraction of brighter area increases while that of the darker area decreases. Consequently, the total brightness increases. This illustrates that a rough Lambertian surface modeled as Figure 1a is non-Lambertian in reflectance, i.e. for fixed θ_i, the reflectance DOES change as the observer moves.

Thus in the Oren model, the reflectance of each S_k depends on R, the angles of incidence (θ_i, ϕ_i) and reflection (θ_r, ϕ_r), σ^2, $\alpha = max[\theta_r, \theta_i]$, $\beta = min[\theta_r, \theta_i]$, and statistical fitting parameters $\delta = 0.33$, $\epsilon_1 = 0.09$ and $\epsilon_2 = 0.13$. These parameters were obtained via a functional approximation as described in [4]. The model includes a factor K_1 which accounts for direct reflection from the facets and K_2 for the interreflection between adjacent facets. The result in [4] (dropping subscripts k on the angles) is

$$\sigma_k^0 = \frac{R}{\pi} cos\theta_i (K_1 + K_2) \tag{4}$$

where

$$K_1 = C_1 + cos(\phi_r - \phi_i) C_2 tan\beta \tag{5}$$

$$+ \quad (1 - |cos(\phi_r - \phi_i|) C_3 tan\left(\frac{\alpha+\beta}{2}\right) \tag{6}$$

and the coefficients C_i are defined as:

$$C_1 = 1 - 0.5\frac{\sigma^2}{\sigma^2 + \delta} \tag{7}$$

$$C_2 = 0.45\frac{\sigma^2}{\sigma^2 + \epsilon_1} sin\alpha \tag{8}$$

if $cos(\phi_r - \phi_i) \geq 0$,

$$C_2 = 0.45\frac{\sigma^2}{\sigma^2 + \epsilon_1}(sin\alpha - (2\beta/\pi)^3) \tag{9}$$

if $cos(\phi_r - \phi_i) < 0$,

$$C_3 = 0.125\frac{\sigma^2}{\sigma^2 + \epsilon_1}\frac{4\alpha\beta}{\pi^2} \tag{10}$$

$$K_2 = 0.17\frac{R^2}{\pi}\frac{\sigma^2}{\sigma^2 + \epsilon_2}\left[1 - cos(\phi_r - \phi_i)\left(\frac{2\beta}{\pi}\right)^2\right] \tag{11}$$

A simplified model neglects K_2, C_3 and uses one equation for C_2 to obtain

$$K_1 = C_1 + C_2 tan\beta max[0, cos(\theta_r - \theta_i)] \tag{12}$$

Note that when the variance $\sigma^2 = 0$, the model of [4] reduces to the Lambertian model.

From numerical evalations in [4], we see that σ_k^0 increases as the viewing direction approaches the source direction. In the backward (source) direction σ_k^0 is maximum and gets cut off due to strong masking effects when $\theta_r > \theta_i$. In the forward direction, interreflections dominate since most facets are self-shadowed so that the visible facets receive radiation primarily from adjacent facets.

III. RESULTS FROM MODEL AND MEASUREMENTS

In this section, we compare σ_k^0 obtained by measurement with those predicted by the two models. The measured results were obtained using the data and methods of [5]. The model results assume that all facets on the mountain slope have a constant value of R which was chosen for best fit with the measurements.

Figure 2 shows a perspective view of the topography. The map covers locations $(x, y) = (-6310, 4500)$ to $(4290, 9500)$ meters with transmitter and receiver coordinates off the map at locations $(x, y) = (0, 0)$ and $(2035, -1272)$ respectively. The values of $\theta_i, \theta_r, \phi_i, \phi_r$ are determined for each S_k. The measured reflectivity of each S_k is represented by the grey scale of the boundary lines. The main reflection is seen to be the steep mountain slope where the angle of incidence and reflection are approximately equal. A figure for the model reflectivity is similar.

The differences between model and measurements are difficult to see without color, since the folds in the terrain compete with the reflection intensity grey scale. Thus we consider a top view of the topography looking straight down where the S_k appear uniformly spaced on the (x, y) grid. Figure 3 shows the contour lines of the topography viewed from above, and Figure 4 shows the corresponding measured reflectivity. The scale is relative, and has not been calibrated to absolute values of σ_k^0. The reflectance predicted using the Oren

scattering model is shown in Figure 5, and using the Lambertian model in Figure 6. In Figures 4 and 5, the white areas are not visible from the transmitter or receiver. It is clear that the Oren model results correspond more closely with the measurements than the Lambertian model.

We also compare the measured and model reflectivities of each S_k as a function of θ_i. Figure 7 shows that the Oren reflectivities are spread over a range of values due to the dependence on θ_r and $\phi_r - \phi_i$ in (4)-(11). This spread is narrowed with decreasing σ^2 to become a single Lambertian curve (3) for $\sigma^2 = 0$. Figure 8 shows that the measured results are spread in a fashion similar to the Oren model. The correlation coefficient of the σ_k^0 of the measurements and model is 0.80 for the Lambertian model and 0.88 for the Oren model.

The predicted impulse response $|h(t)|^2$ for the Oren model is compared with the measured response in Figure 9. These preliminary results, over a limited range of delays determined by the map area of Figure 3, show that the Oren model prediction agree well with the measurements.

IV. SUMMARY

The results show that the Oren scattering model [4] can be used successfully to predict the impulse response in mountainous terrain using only two parameters: the albedo of a triangular patch of terrain, and the variance of the orientation of the facets within the patch with respect to its normal. The Oren model with a variance of zero reduces to the Lambertian model. The results show good agreement using only a single value of these parameters for all terrain patches. Thus, in mountainous terrain, it may not be necessary to further refine the model by choosing different parameters for each patch, depending on the ground cover and mineral content. However, it remains to be determined if objects on the mountain slopes such as buildings or metal objects have a significant effect on the predicted impulse response.

APPENDIX A
CROSS-ARRAY SIGNAL PROCESSING

Consider two set of linear arrays crossing each other, the centers of the horizontal and vertical sub-arrays being coincident and consisting of M and N sensors spaced equally at a distance d.

The wavelength is equal to $\lambda = \frac{c}{f_0}$, where c is the speed of light and f_0 is the frequency of the wave. Assuming the reference phase of the center sensor $x_{\frac{M-1}{2}}$ or $y_{\frac{N-1}{2}}$ is taken to be zero, the wavefront reaches the element x_0 before element x_1 by a distance equal to $d\cos\alpha$, and the difference in the phase is $\frac{2\pi d\cos\alpha}{\lambda}$. The phase of $y_{\frac{N-3}{2}}$ advances the phase of the center sensor by $\frac{2\pi d\sin\alpha}{\lambda}$.

Let s be a directional vector corresponding to the DOA of the wavefront be α, then we have

$$s(\alpha) = \begin{bmatrix} e^{-j\frac{\pi d\cos\alpha}{\lambda}(M-1)} \\ e^{-j\frac{\pi d\cos\alpha}{\lambda}(M-3)} \\ \cdot \\ 1 \\ \cdot \\ e^{j\frac{\pi d\cos\alpha}{\lambda}(M-3)} \\ e^{j\frac{\pi d\cos\alpha}{\lambda}(M-1)} \\ e^{-j\frac{\pi d\sin\alpha}{\lambda}(N-1)} \\ e^{-j\frac{\pi d\sin\alpha}{\lambda}(N-3)} \\ \cdot \\ \cdot \\ \cdot \\ e^{j\frac{\pi d\sin\alpha}{\lambda}(N-3)} \\ e^{j\frac{\pi d\sin\alpha}{\lambda}(N-1)} \end{bmatrix} \tag{13}$$

Let w be a weight vector $w = [w_0, w_1, ...w_{M+N-1}]^H$, and let u be a received vector

$$u = [x_0, x_1, \cdots, x_{M-1}, y_0, y_1, \cdots, y_{N-1}]^H$$

For the conventional beamforming method the power spectrum as a function of DOA α is given by

$$S_{BF}(\alpha) = s^H(\alpha)Rs(\alpha) \tag{14}$$

where R is the (N+M)x(N+M) correlation matrix $R = E[uu^H]$.

For the MVDR technique we introduce a constraint condition

$$w^H s(\alpha_0) = 1$$

The optimization criterion is to minimize the average energy of the array output $z = w^H u$. It is easy to show that the optimum weight w is

$$w = \frac{R^{-1}s(\alpha_0)}{s^H(\alpha_0)R^{-1}s(\alpha_0)}$$

The MVDR spectrum for the cross-array is given by

$$S_{MVDR} = \frac{1}{s^H(\alpha)R^{-1}s(\alpha)} \tag{15}$$

Spatial smoothing and phase drift corrections are described in [12].

REFERENCES

[1.] Braun, W.R. and U. Dersch, "A physical mobile radio channel model", IEEE T-Vehic. Tech., 40, No. 2, pp. 472-482, May 1991.

[2.] Lebherg, M., W. Wiesbeck and W. Krank, "A versatile wave propagation model for the VHF/UHF range considering three-dimensional terrain", IEEE Trans. Antennas and Propagation, vol. 40, pp. 1121-1131, 1992.

[3.] Beckmann, P. and A. Spizzichino, *The scattering of electromagnetic waves from rough surfaces*, Pergamon Press, 1963.

[4.] Oren, M. and S.K. Nayar,"Generalization of the Lambertian model and implications for machine vision", *International Journal of Computer Vision*, February 1994.

[5.] Kirlin, R.L, P.F. Driessen, "Relationship between measured 900 MHz complex impulse responses and topographical map data", *Proc. IEEE Vehic. Tech. Conf.*, pp. 1811-1815, 1994.

[6.] Driessen, P.F., "Multipath delay characteristics in mountainous terrain at 900 MHz", *Proc. IEEE Vehic. Tech. Conf.*, pp. 520-523, 1992.

[7.] Driessen, P.F., "Multipath delay characteristics in mountains terrain -comparison of theoretical predictions with measurement results", *Proc. IEEE Vehic. Tech. Conf.*, pp. 606-609, 1991.

[8.] Driessen, P.F., "Multipath delay characteristics in mountainous terrain in 900 MHz", *Proc. IEEE Vehic. Tech. Conf.*, pp. 606-609, 1990.

[9.] Broschat, S.L., E.I. Thorsos, A. Ishimaru, "A heuristic algorithm for the bistatic radar cross section for random rough surface scattering", *IEEE Trans Geoscience and Remote Sensing*, vol. 28, No. 2, pp. 202-206, March 1990.

[10.] Ulaby, F.T., Dobson, M.C., *Handbook of Radar Scattering Statistics for Terrain*, Artech House, 1988.

[11.] Fung, A.K., *Microwave Scattering and Emission Models and their Applications*, Artech House, 1994.

[12.] Kirlin, R.L., "Multipath channel modelling in mobile telecommunications"., *Final Report* to Communications Canada, Spectrum Engineering, Ottawa, Canada, October 1992.

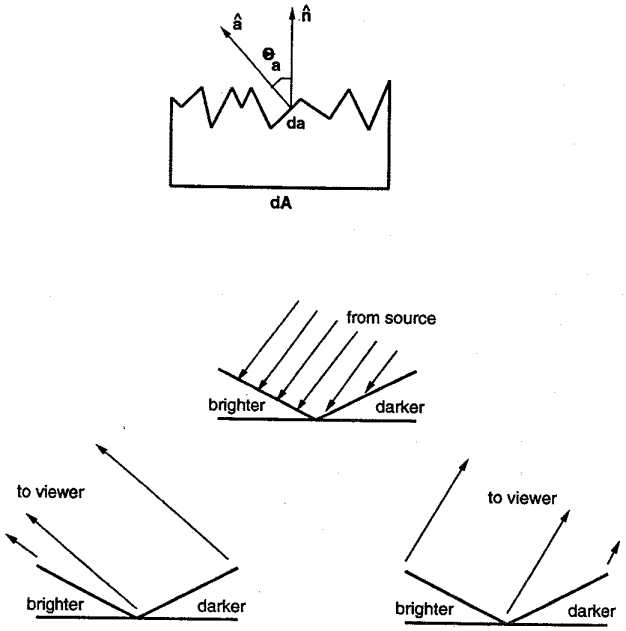

Figure 1
Surface modeled as a collection of V-cavities

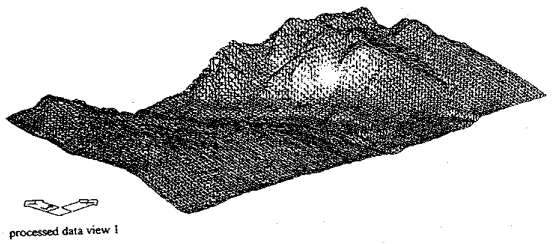

Figure 2
Perspective view of terrain

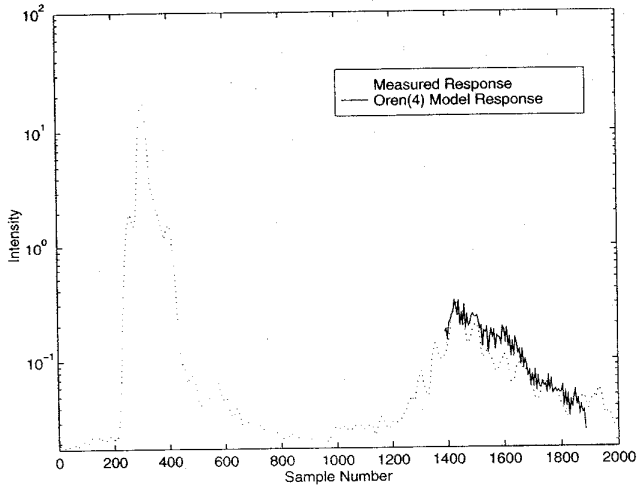

Figure 9
Measured and predicted impulse response

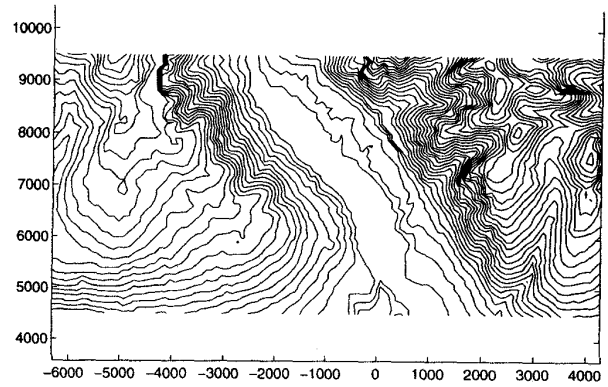

Figure 3
Terrain contours

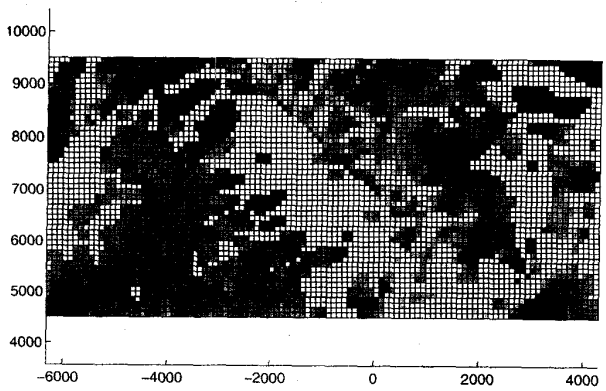

Figure 4
Measured reflectivities

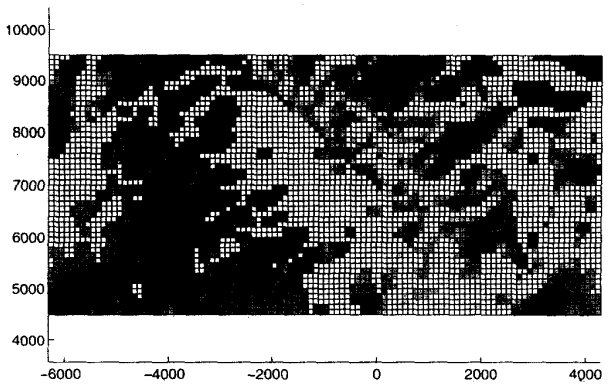

Figure 5
Oren model reflectivities

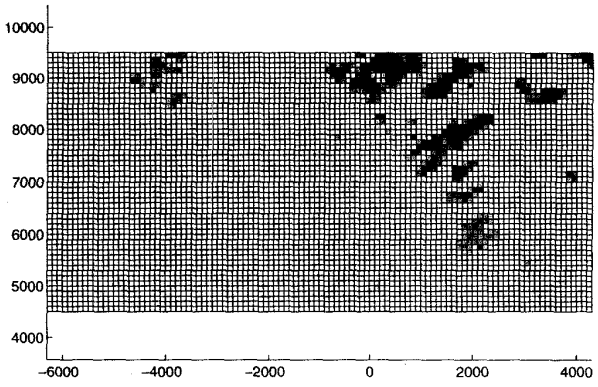

Figure 6
Lambertian model reflectivities

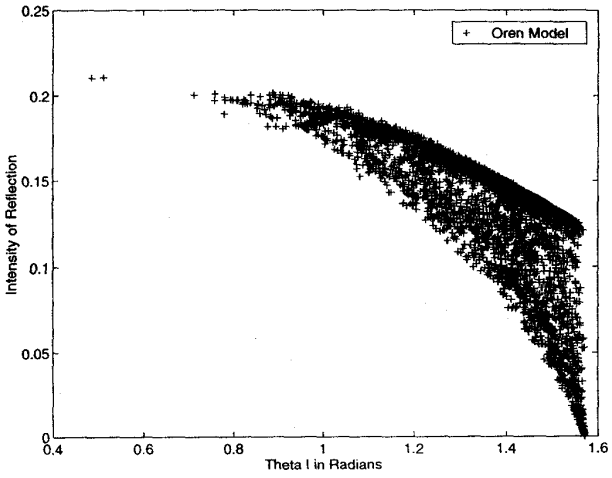

Figure 7
Oren model reflectivities versus angle of incidence θ_i

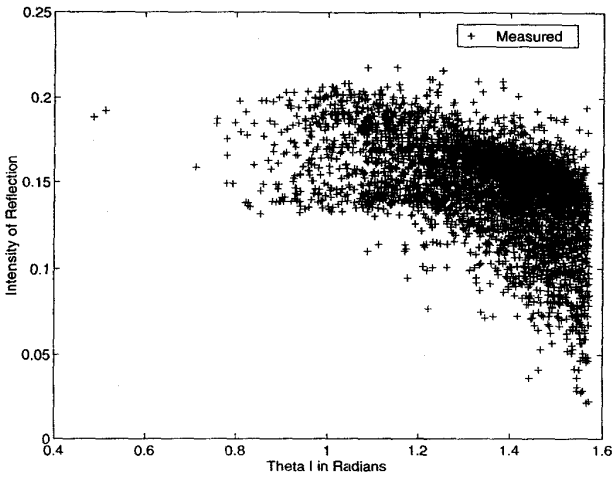

Figure 8
Measured reflectivities versus angle of incidence θ_i